Deubiquitinase UCHL1 Maintains Protein Homeostasis through the PSMA7–APEH–Proteasome Axis in High-grade Serous Ovarian Carcinoma

Apoorva Tangri[1], Kinzie Lighty[1], Jagadish Loganathan[1], Fahmi Mesmar[2], Ram Podicheti[3], Chi Zhang[4], Marcin Iwanicki[5], Ronny Drapkin[6], Harikrishna Nakshatri[7,8], and Sumegha Mitra[1,8]

ABSTRACT

High-grade serous ovarian cancer (HGSOC) is characterized by chromosomal instability, DNA damage, oxidative stress, and high metabolic demand that exacerbate misfolded, unfolded, and damaged protein burden resulting in increased proteotoxicity. However, the underlying mechanisms that maintain protein homeostasis to promote HGSOC growth remain poorly understood. This study reports that the neuronal deubiquitinating enzyme, ubiquitin carboxyl-terminal hydrolase L1 (UCHL1), is overexpressed in HGSOC and maintains protein homeostasis. UCHL1 expression was markedly increased in HGSOC patient tumors and serous tubal intraepithelial carcinoma (HGSOC precursor lesions). High UCHL1 levels correlated with higher tumor grade and poor patient survival. UCHL1 inhibition reduced HGSOC cell proliferation and invasion, as well as significantly decreased the *in vivo* metastatic growth of ovarian cancer xenografts. Transcriptional profiling of UCHL1-silenced HGSOC cells revealed downregulation of genes implicated with proteasome activity along with upregulation of endoplasmic reticulum stress–induced genes. Reduced expression of proteasome subunit alpha 7 (PSMA7) and acylaminoacyl peptide hydrolase (APEH), upon silencing of UCHL1, resulted in a significant decrease in proteasome activity, impaired protein degradation, and abrogated HGSOC growth. Furthermore, the accumulation of polyubiquitinated proteins in the UCHL1-silenced cells led to attenuation of mTORC1 activity and protein synthesis, and induction of terminal unfolded protein response. Collectively, these results indicate that UCHL1 promotes HGSOC growth by mediating protein homeostasis through the PSMA7–APEH–proteasome axis.

Implications: This study identifies the novel links in the proteostasis network to target protein homeostasis in HGSOC and recognizes the potential of inhibiting UCHL1 and APEH to sensitize cancer cells to proteotoxic stress in solid tumors.

Introduction

Cancer cells maintain protein homeostasis to sustain their high proliferating state. Protein synthesis is intrinsically an error-prone process, and up to 30% of newly synthesized misfolded proteins are degraded immediately after protein translation (1, 2). Moreover, cancer cells with profound chromosomal instability, mutations, and physiologic stressors carry the burden of excessive protein production, mutant proteins with stoichiometrically altered protein complexes, and increased misfolded and damaged proteins (3–5). Together, this contributes to a proteotoxic state in cancer cells if misfolded, unfolded, and damaged proteins are not efficiently removed (2, 4–6). Therefore, understanding the mechanisms that regulate protein homeostasis is an essential link to develop effective treatment strategies. Disrupting this equilibrium through the use of proteasome inhibitors has already revolutionized the treatment of hematologic malignancies, such as multiple myeloma and mantle cell lymphoma (7). However, the first-generation proteasome inhibitor, bortezomib, has shown limited success in solid tumors (7), suggesting the need for alternative approaches to specifically target protein homeostasis in solid tumors.

The ubiquitin-proteasome system is at the core of the protein quality control network and works together with protein folding and protein clearance pathways to maintain protein homeostasis (2, 5). Most cancer cells display enhanced proteasome activity to maintain the integrity of the onco-proteome; regulate cellular levels of proteins, like cell-cycle checkpoints or tumor suppressors; and avoid growth arrest due to the accumulation of misfolded proteins (7, 8). Proteasome inhibition induces an integrated stress response as a result of amino acids and ubiquitin deprivation, reduced protein synthesis, and increased endoplasmic reticulum (ER) stress, which induces terminal unfolded protein response (UPR; refs. 9–11). It is now clear that cancer cells adapt in various ways to maintain protein homeostasis and enhance proteasome activity through upregulation of proteasome subunits, proteasome activators, or proteasome assembly factors (12–15), which makes them fascinating selective targets to block proteasome activity in cancer cells. Emerging in this field are deubiquitinating enzyme (DUB) inhibitors (16). A pan-DUB inhibitor has been reported to sensitize breast cancer cells to the proteotoxicity caused by oxidative stress in the absence of glutathione (16). Moreover,

[1]Department of Obstetrics and Gynecology, Indiana University School of Medicine, Indianapolis, Indiana. [2]Department of Intelligent Systems Engineering, Indiana University, Bloomington, Indiana. [3]Center for Genomics and Bioinformatics, Indiana University, Bloomington, Indiana. [4]Department of Medical and Molecular Genetics, Indiana University School of Medicine, Indianapolis, Indiana. [5]Department of Chemistry and Chemical Biology, Stevens Institute of Technology, Hoboken, New Jersey. [6]Perelman School of Medicine, University of Pennsylvania, Philadelphia, Pennsylvania. [7]Department of Surgery, Indiana University School of Medicine, Indianapolis, Indiana. [8]Indiana University Simon Comprehensive Cancer Center, Indianapolis, Indiana.

Note: Supplementary data for this article are available at Molecular Cancer Research Online (http://mcr.aacrjournals.org/).

A. Tangri and K. Lighty contributed equally to this article.

Corresponding Author: Sumegha Mitra, OB-GYN, Indiana University Health, 980 W Walnut St, Indianapolis, IN 46202. Phone: 317-274-3967; Fax: 317-944-7417; E-mail: mitras@indiana.edu

Mol Cancer Res 2021;19:1168–81

doi: 10.1158/1541-7786.MCR-20-0883

the small-molecule inhibitor of proteasome-associated DUBs, b-AP15, has been reported to overcome bortezomib resistance, inducing proteotoxic stress and reactive oxygen species (17). These studies demonstrated the effect of global DUB inhibition on proteotoxic stress–induced cancer cell death. However, the knowledge of a specific DUB remains elusive.

Ubiquitin carboxyl-terminal hydrolase L1 (UCHL1) is a neuronal DUB that constitutes about 1% to 2% of total brain proteins (18). The loss of UCHL1 has been implicated in the accumulation of neuronal protein aggregates because of impaired proteasomal degradation in neurodegenerative diseases (19, 20). Although UCHL1 is overexpressed in several malignancies (21–23), nothing is known about its role in the protein clearance pathway in cancer. UCHL1 plays a promiscuous role in cancer and has been shown to promote metastatic growth by its deubiquitinating activity associated with hypoxia-inducible factor-1α (HIF1α), cyclin B1, and TGFβ receptor 1 (21, 22, 24), while it is also reported as an epigenetically silenced tumor suppressor gene in some cancers (25, 26). In this study, we report that increased expression of UCHL1 in high-grade serous ovarian cancer (HGSOC) mediates protein homeostasis. HGSOC is the most prevalent and lethal histotype of ovarian cancer. It is characterized by chromosomal instability; germline or somatic mutations, including mutations in the tumor suppressor gene *TP53*; DNA damage; oxidative stress; and high metabolic demand that exacerbate misfolded, unfolded, and damaged protein burden (27). However, not much is known about the mechanisms that promote proteostasis in HGSOC. Here, we show that UCHL1 mediates protein homeostasis through increased expression of acylaminoacyl peptide hydrolase (APEH) and proteasome subunit alpha 7 (PSMA7), resulting in increased proteasomal activity and protein degradation. Furthermore, UCHL1 inhibition results in the accumulation of polyubiquitinated proteins leading to the induction of terminal UPR and attenuation of mTOR complex 1 (mTORC1) activity and protein synthesis. This is perhaps the first report to establish the role of UCHL1 in mediating protein homeostasis through the PSMA7–APEH–proteasome axis and identifies the novel druggable links to target protein homeostasis in HGSOC.

Materials and Methods

Cell culture

All ovarian cancer cell lines were maintained in 10% DMEM (Corning, catalog no., 10-013-CV) supplemented with 1% nonessential amino acid, 1% vitamins, and 1% penicillin/streptomycin (Corning). Fallopian tube epithelial cells were obtained from R. Drapkin and cultured in DMEM-Ham F12 Media (Corning) supplemented with 2% UltroserG (Crescent Chemical Company). Nonciliated fallopian tube epithelial (FNE) cells transfected with vector pWZL-mutant p53-R175H were maintained in WIT-Fo culture media from Live Tissue Culture Service Center, University of Miami (Miami. FL) by the laboratory of M. Iwanicki. Human primary mesothelial cells and fibroblasts isolated from the omentum of a healthy woman were obtained from Dr. Anirban Mitra (Indiana University, Indianapolis, IN), and were grown in 10% DMEM. All cell lines were authenticated by short tandem repeat profiling and were negative for *Mycoplasma* contamination.

Patient samples and patient data analysis

Frozen human serous ovarian cancer primary tumors and matched normal adjacent fallopian tubes were obtained from the tissue bank of Indiana University Simon Cancer Center (Indianapolis, IN). The study was approved by the Institutional Regulatory Board of Indiana University (Indianapolis, IN, protocol nos. 1106005767 and 1606070934). Human serous tubal intraepithelial carcinomas (STIC) tissue slides ($n = 3$) were obtained from R. Drapkin, and the study was approved by the Institutional Regulatory Board of University of Pennsylvania (Philadelphia, PA). Written informed consent was obtained from all the patients, and only deidentified patient specimens were used. The studies were conducted in accordance with the Belmont Report. Tissue microarrays (TMA) of HGSOC tumors with normal ovary (OV1502 and BC11012) and normal fallopian tube (UTE601) were purchased from US Biomax Inc and were processed at the same time. The Cancer Genome Atlas (TCGA) database was analyzed using the Oncomine gene browser (28) to examine gene expression in patients with HGSOC and across cancer stages and tumor grades. Survival analysis of patients with HGSOC ($n = 1{,}104$) who had received chemotherapy after optimal or suboptimal debulking was performed using the Kaplan-Meier plotter (29). Survival analysis of patients with HGSOC was analyzed in an in-house cohort of Molecular Therapeutics for Cancer, Ireland(MTCI) and GSE9899 ($n = 244$) using OVMARK (30). Patients with no residual tumors and UCHL1 median expression were used as the cutoff. Correlation between UCHL1 and p53 expression levels in patients with HGSOC with *TP53* mutations (putative driver, $n = 92$; missense mutation, $n = 143$; and no mutation, $n = 10$) was analyzed in TCGA database using cBioPortal (31).

Animal study

The animal study was performed according to protocols approved by the Animal Care and Use Committee of Indiana University (Indianapolis, IN). A total of 5×10^6 OVCAR8 cells were intraperitoneally injected into 5- to 6-week-old female athymic nude mice (Envigo) as described previously (32). Mice were randomized into two groups: vehicle control and LDN57444 (10 mice/group). After 10 days of injecting the cancer cells, mice were intraperitoneally injected with LDN57444 (1 mg/kg) or 25% DMSO thrice per week for 5 weeks. All the mice were euthanized after 45 days of injecting the cells.

Methylated DNA immunoprecipitation

Methylated DNA immunoprecipitation (MeDIP) was performed using the Active Motif Kit (catalog no. 55009). The genomic DNA was isolated from the ovarian cancer cell lines using the DNeasy Blood and Tissue Kit (Qiagen). DNA (20 ng/μL) was sheared on ice for three pulses of 10 seconds at 30% amplitude with a 20-second pause between each pulse using a tip probe sonicator. DNA fragment size was ensured by Agilent TapeStation. MeDIP was performed using the 5-methylcytosine antibody or control mouse IgG according to the manufacturer's protocol. Quantitative PCR was performed in the input and MeDIP samples for UCHL1 promoter using the following primers: forward: ccgctagctgtttttcgtct and reverse: ctcacctcggggttgatct. The analysis was performed as a percentage of input normalized to control IgG. Amplicons were resolved using a 2% agarose gel.

Chromatin immunoprecipitation

Chromatin immunoprecipitation (ChIP) was carried out using the ChIP-IT Express Kit (Active Motif, catalog no. 53008). Briefly, cells were fixed in 1% Methanol-free Formaldehyde (Thermo Fisher Scientific, catalog no. 28908), followed by glycine-stop fix solution treatment. Cells were lysed as per the manufacturer's protocol. The nuclei were suspended in the shearing buffer and sonicated for eight cycles of 30-second on/off using Bioruptor Pico (Diagenode). The sheared chromatin was reverse cross-linked and DNA fragment size was ensured by Agilent TapeStation. ChIP was performed according to

the manufacturer's protocol using an anti-histone H3K4 trimethyl antibody (Abcam, ab8580) or control IgG. Quantitative PCR was performed for UCHL1 promoter using the following primers: ccgctagctgtttttcgtct and ctcacctcggggttgatct. The analysis was performed using the $2^{-\Delta\Delta C_t}$ method (33).

Cell proliferation and colony formation assay

Cell proliferation was measured by MTT assay as described previously. A total of 2,000 cells transfected with control or target-specific siRNA per well were plated in the 96-well plate and MTT assay was performed after day 4. The reduction of MTT into purple color formazan was measured at 560 nm and adjusted for background absorbance at 670 nm. Colony formation assay was performed by plating 1,000 cells per well in the 6-well plate. The colonies were allowed to grow for 8 to 10 days and the fixed colonies were stained with 0.05% crystal violet solution. The colonies were imaged and counted using ImageJ.

Spheroid culture of FNE cells and LDN57444 treatment

FNE cells transfected with pWZL-p53-R175H ($FNE^{mutp53\text{-}R175H}$), to overexpress mutant p53 variant R175H and GFP, were seeded in Ultra-low Adhesion Plates (Corning). Matrigel (2%) was added to the suspended culture after 24 hours to support basement membrane adhesion. After 4 days, the three-dimensional (3D) structures of $FNE^{mutp53\text{-}R175H}$ cells were treated with DMSO or UCHL1 inhibitor, LDN57444 (10 μmol/L, 5 days). Subsequently, cellular clusters were treated with 2 μmol/L ethidium bromide (EtBr) and imaged. EtBr incorporation was measured as the number of red channel pixels within cellular clusters as described previously (34).

Organotypic 3D culture model of omentum and invasion assay

The organotypic 3D culture model of the omentum was assembled in a Fluoroblock Transwell Insert (8 μm pore size, BD Falcon) as described previously (35). Briefly, 2×10^5 fibroblasts with collagen I and 2×10^6 primary mesothelial cells isolated from the omentum of a healthy woman were seeded in the transwell insert. After 24 hours, 2×10^5 UCHL1-silenced or unsilenced OVCAR3 (RFP labeled) and Kuramochi (GFP labeled) cells were plated over the omental cells in 200 μL of serum-free DMEM. Cancer cells were allowed to invade for 16 hours after placing the insert in a well of 24-well plate containing 700 μL of 10% DMEM. Invaded cells were fixed, imaged (five fields/insert), and counted.

Determination of proteasome and APEH activity

The chymotrypsin-like proteasome activity was measured by Sigma-Aldrich Kit (catalog no. MAK172) using the fluorogenic substrate, LLVY-R110, as per the manufacturer's protocol and as described previously (36). Total protein (50 μg) from fresh cell lysate or tissue homogenates in even volumes (90 μL) was incubated with 100 μL of proteasome assay buffer containing LLVY-R110 at 37°C. R110 cleavage by proteasomes was measured at 525 nm with excitation at 490 nm. Fluorescence intensity was normalized with the fluorescence of the blank well. APEH activity was measured by chromogenic substrate, acetyl-Ala-pNa (Bachem; ref. 37). Total protein (45 μg) in even volume (100 μL) in 50 mmol/L Tris-HCl buffer pH 7.5 was incubated with acetyl-Ala-pNa at 37°C. The release of p-nitroaniline was measured at 410 nm and was normalized with the absorbance of the blank well.

Immunoblot analysis

Immunoblotting was performed using a standard protocol as described previously (35). Cells were lysed in NP-40 buffer containing Protease and Phosphatase Inhibitors Cocktails (Millipore), 0.2 mmol/L phenylmethylsulfonyl fluoride, and 10 mmol/L N′ ethylmalamide. Protein quantification was conducted using the Pierce BCA Protein Assay Kit (Thermo Fisher Scientific, #23225). Proteins were resolved by 4%–20% gradient SDS-PAGE. Primary antibodies were procured from Cell Signaling Technology: UCHL1 (13179), ATF3 (33593), ATF4 (11845), pSer51 eIF2α (3398), cleaved caspase-3 (9664), pSer235/236 S6 Ribosomal Protein (4858), S6 Ribosomal Protein (2217), 4E-BP1 (9452), and pThr37/46 4E-BP1 (2855). Other antibodies included UCHL1 (MAB6007, R&D Systems), PSMA7 (PA5-22289, Invitrogen), APEH (376612, Santa Cruz Biotechnology), cleaved caspase-3 (AF835, R&D Systems), and actin-HRP (Sigma).

Transfection, transduction, and cell treatments

Gene knockout was carried out by transfecting HGSOC cells with control and target-specific siRNAs (set of four siRNAs) using TransITX2 (Mirus Bio, catalog no. MIR6000). ON-TARGETplus siRNA (Horizon Discovery) for UCHL1 (catalog no. LQ-004309-00-0010), PSAM7 (catalog no. LQ-004209-00-0010), APEH (catalog no. LQ-005785-00-0010), EIF2AK3 (LQ-004883-00-0005), and control (catalog no. D-001810-10-05) were used. UCHL1 knockdown was also carried out by transducing HGSOC cells with control or UCHL1 short hairpin RNA (shRNA) lentiviral virus particles (Santa Cruz Biotechnology, catalog no. sc-108080 and sc-42304-V) using TransDux MAX (System Biosciences, catalog no. LV860A-1). PSMA7-pReceiver-M02 (catalog no. EX-Z7450-M02) and APEH-pReceiver-M02 (catalog no. EX-Z0642-M02) expression vectors were obtained from GeneCopoeia. Plasmids were transfected using FuGENE HD (Promega, catalog no. E2311) as per the manufacturer's protocol. For 5-aza-2′-deoxycytidine (5-aza-DC; Sigma-Aldrich, catalog no. A3656) treatment, cells were plated at a low density and the next day, were treated with 5-aza-DC (5 μmol/L, 48 hours) to allow its incorporation into the DNA of the dividing cells (38).

IHC

IHC was performed by IU Health Pathology Laboratory. Briefly, slides were baked at 60°C for 30 minutes before the standard deparaffinization procedure, followed by blocking of endogenous peroxides and biotin. Antigen retrieval was performed using 10 mmol/L citrate buffer, pH 6 at 95°C, followed by 1 hour blocking and incubation with preoptimized primary anti-UCHL1 (MAB6007, R&D Systems) or anti-p53 (Dako) antibodies (1:200 dilution). TMA slides were digitally scanned by Aperio ScanScope CS Slide Scanner (Aperio Technologies) and staining was quantified in three intensity ranges: weak, 0 to 100; positive, 100 to 175; and strong, 175 to 220. TMA slides were also hand-scored by Dr. George Sandusky (Department of Pathology, Indiana University School of Medicine) as 1 being a weak expression, 2 moderate, 3 strong, and 3+ very strong.

Assay for transposase-accessible chromatin sequencing

Assay for transposase-accessible chromatin sequencing (ATAC-seq) was performed by the Center for Medical Genomics, Indiana University School of Medicine (Indianapolis, IN). The Tagment DNA TDE1 enzyme and Nextera DNA Flex Library Prep Kit (Illumina, catalog no., 15027866 and 15027865) were used. Briefly, 1×10^5 OVCAR3 and SKOV3 cells were lysed in a nonionic detergent to yield pure nuclei. The chromatin was fragmented and simultaneously tagmented with the sequencing adaptor using Tn5 transposase to generate ATAC-seq libraries, which were sequenced on NextSeq 500 (Illumina) with NextSeq75 High Output v2 Kit (Illumina, catalog no. FC-404-2005). Raw fastq files were aligned to the human

GRCH38 genome by using bowtie 2 (39). MACS2 and ENCODE standardized pipeline and parameters were utilized for peak detection (40). Peaks on the promoter region of the *UCHL1* gene were plotted using the UCSC genome browser (41).

RNA isolation, real-time PCR, and RNA sequencing

Total RNA from cell lines and patient tumors was extracted using the miRNeasy Mini Kit (Qiagen, catalog no., 217004). Real-time PCR was performed using TaqMan gene expression assays after cDNA preparation using the High-capacity Reverse Transcription Kit (Applied Biosystems, catalog no. 4368814). β-actin and tata-box binding protein (TBP) were used as endogenous controls. For RNA sequencing, 1 μg of total RNA was used for library preparation using the TruSeq Stranded mRNA Kit (Illumina, catalog no. RS-122-2103) after rRNA depletion using Ribo-Zero Plus (Illumina, catalog no. 20037135). RNA sequencing (RNA-seq) was performed using NextSeq75 High Output v2 Kit and NextSeq 500 (Illumina, catalog no. FC-404-2005). Using TruSeq 3′ SE adaptor sequence, AGATCGGAAGAGCACACGTCTGAACTCCAGTCAC, RNA-seq reads were trimmed and were then mapped to the gene regions in a strand-specific manner using htseq-count (version 0.5.4p1; ref. 42). RNA-seq data have been made available to the public, Gene Expression Omnibus accession no. GSE168935. Differentially expressed genes at 5% FDR with at least 2-fold change were called using DESeq2 ver.1.12.3 as described previously (43).

Statistical analysis

Statistical significance was calculated using Student *t* test and one-way ANOVA using Prism 8.0. The log-rank test was used to determine the significance of survival analysis. All results are expressed as mean ± SD from three biological repeats, unless otherwise stated. The *P* value of less than 0.05 was considered significant.

Results

UCHL1 overexpression is an early event in HGSOC and associates with poor patient prognosis

To assess the role of UCHL1 in HGSOC, we examined publicly available TCGA data of patients with serous ovarian cancer. Our analysis of TCGA data revealed that *UCHL1* is a frequently overexpressed gene in patients with HGSOC. UCHL1 mRNA levels were significantly high in primary and recurrent tumors compared with normal ovaries (**Fig. 1A**). Moreover, UCHL1 expression was markedly elevated in patients with HGSOC with advanced-stage and higher grade tumors compared with grade 1 and stage 1 tumors, respectively (**Fig. 1B** and **C**). To confirm these results at the protein level, we performed UCHL1 IHC staining in TMAs consisting of HGSOC tumors, normal ovaries, and normal fallopian tubes. Compared with normal tissues, UCHL1 expression was significantly higher in HGSOC tumors (**Fig. 1D** and **E**). UCHL1 staining was positive in 78.4% (69/88) of tumors and its expression was high in 59.1% (52/88) of tumors, whereas its expression was negligible or low in the normal fallopian tubes and ovaries, respectively. Furthermore, UCHL1 mRNA and protein levels were elevated in primary tumors compared with their matched normal adjacent fallopian tube (**Fig. 1F**, paired samples). These results suggest that UCHL1 expression is upregulated in HGSOC. To test whether UCHL1 expression is an early event in HGSOC, we performed UCHL1 IHC staining in STIC. HGSOC is known to originate from the lesions in fallopian tube known as STICs. Mutation in the *TP53* gene is an early event in the development of STICs and the presence of identical *TP53* mutations in the concurrent HGSOC established their clonal relationship (44). UCHL1 expression was significantly elevated in STICs (**Fig. 1G**). Increased UCHL1 staining was observed in the epithelial cells and the associated invasive carcinoma with diffused p53 nuclear staining (**Fig. 1G**), while the UCHL1 staining was absent in p53-negative regions and normal human fallopian tube (**Fig. 1G**; Supplementary Fig. S1A and S1B). Hematoxylin and eosin staining indicated FTE, STIC, and invasive carcinoma (**Fig. 1G**; Supplementary Fig. S1B). Next, to determine the prognostic significance of UCHL1, we analyzed the transcriptomic datasets of patients with HGSOC. Survival analysis using the Kaplan–Meier plotter revealed a significant association of high UCHL1 levels with poor progression-free survival of patients with HGSOC after chemotherapy and debulking (**Fig. 1H**). Moreover, high UCHL1 levels were associated with poor disease-free survival of patients with HGSOC after optimal debulking in GSE9899 and an in-house cohort of MTCI using OVMARK (**Fig. 1I**). Overall, these results indicate that UCHL1 expression in HGSOC patient tumors is an early event and predicts poor prognosis.

Epigenetic upregulation of UCHL1 promotes HGSOC growth

To understand the role of UCHL1 in HGSOC pathobiology, we examined the expression of UCHL1 in a panel of ovarian cancer cell lines (45) characterized as HGSOC and non-HGSOC. Compared with non-HGSOC, UCHL1 mRNA and protein levels were significantly higher in HGSOC cell lines (**Fig. 2A**). Interestingly, the elevated UCHL1 levels in HGSOC cells varied with the different *TP53* mutations and mutant p53 expression levels in these cell lines (**Fig. 2A** and **B**). Similarly, a weak correlation ($r = 0.2$) was seen between UCHL1 and mutant p53 expression levels in patients with HGSOC with missense *TP53* mutations (Supplementary Fig. S2A). In contrast, UCHL1 expression was low or absent in the non-HGSOC cells with wild-type p53 or p53 null, respectively (**Fig. 2A** and **B**). These results confirm our patient data and suggest that UCHL1 expression is not epigenetically silenced in HGSOC as reported in many malignancies (25, 26). Analysis of *UCHL1* gene methylation, quantified as beta value, in the patient tumors in TCGA methylation data revealed hypomethylation (mean beta value = 0.082) at *UCHL1* gene loci (Supplementary Fig. S2B). To test this, we performed MeDIP using the 5-methylcytosine antibody in Kuramochi and OVCAR3 (HGSOC) and HeyA8 and OVCAR5 (non-HGSOC) cells. No enrichment of methylated DNA in the UCHL1 promoter was observed in HGSOC cells, while significant enrichment was observed in non-HGSOC cell lines (**Fig. 2C**; Supplementary Fig. S2C). To further investigate these results at the chromatin level, we performed ChIP using the antibody against histone H3 trimethyl lysine 4 (H3K4me3) and ATAC-seq. ChIP assay revealed enhanced enrichment of H3K4me3 in the UCHL1 promoter in HGSOC cells, OVCAR3 and OVCAR4 (**Fig. 2D**). However, no such enrichment of H3K4me3 was observed in the UCHL1 promoter in SKOV3 cells (**Fig. 2D**). Furthermore, open chromatin marks at the *UCHL1* gene promoter (chromosome 4; region 41257000–41258000; exon 1 to exon 3) were revealed by ATAC-seq analysis of OVCAR3 cells, unlike the non-HGSOC, SKOV3 cells (**Fig. 2E**). To further corroborate these results, we next treated HGSOC and non-HGSOC cell lines with DNA methyltransferase inhibitor, 5-aza-DC. No change in UCHL1 expression was observed in HGSOC cell lines upon treatment with 5-aza-DC (Supplementary Fig. S2D), while UCHL1 expression was increased many folds in non-HGSOC cell lines (Supplementary Fig. S2E). Similarly, 5-aza-DC treatment in fallopian tube epithelial cells demonstrated a significant increase in UCHL1 (Supplementary Fig. S2F). Collectively, the data indicate hypomethylation in the *UCHL1* gene promoter and its epigenetic upregulation in HGSOC.

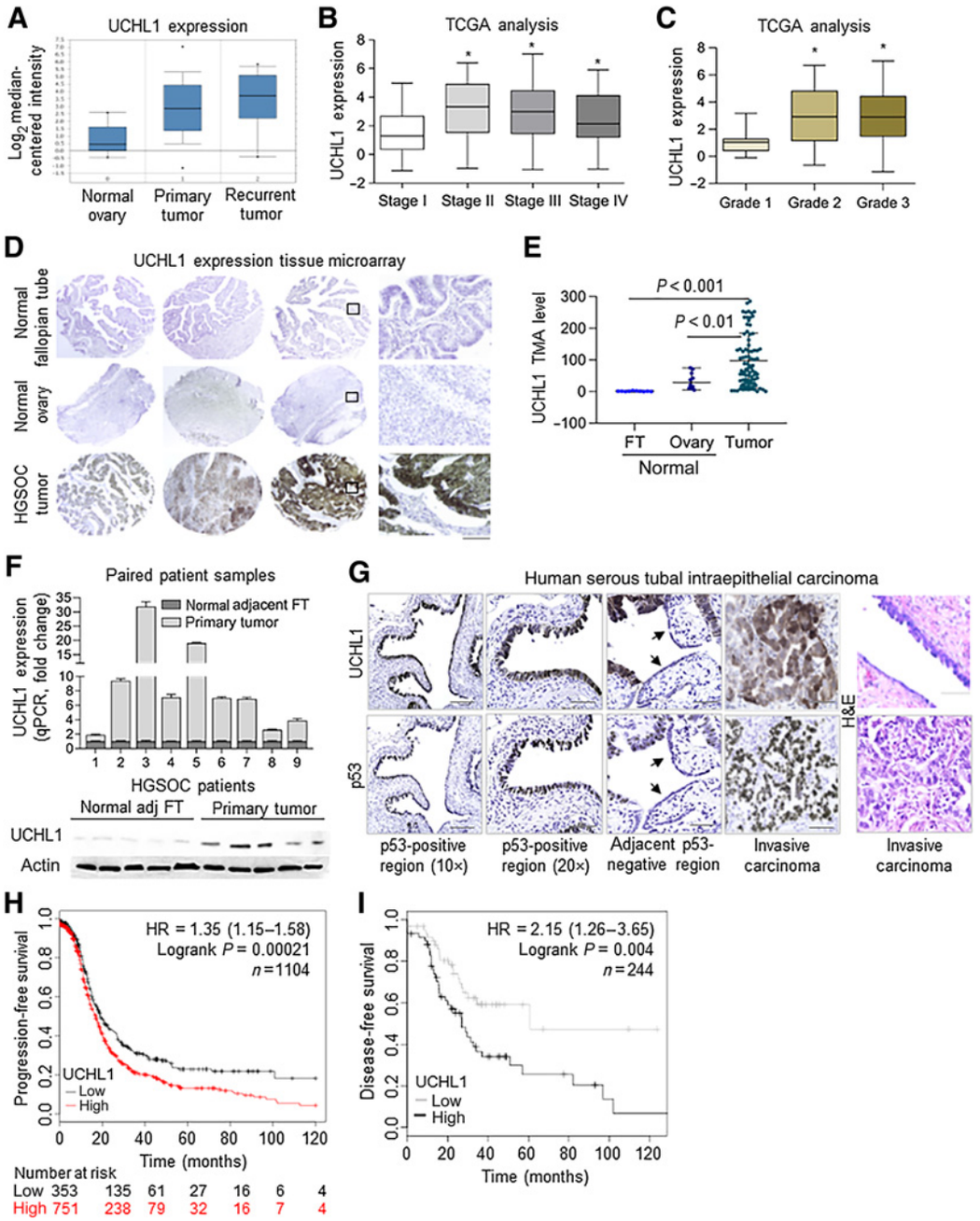

Figure 1.

Increased UCHL1 expression confers poor prognosis in patients with HGSOC. **A,** UCHL1 mRNA expression in primary and recurrent tumors of patients with HGSOC in TCGA database analyzed using Oncomine gene browser. **B,** UCHL1 expression in stage I ($n = 16$), stage II ($n = 27$), stage III ($n = 436$), and stage IV ($n = 84$) tumors of patients with HGSOC in TCGA database. **C,** UCHL1 expression in grade 1 ($n = 15$), grade 2 ($n = 69$), and grade 3 ($n = 479$) tumors of patients with HGSOC in TCGA database. **D,** Representative core images for low, medium, and high UCHL1 levels in HGSOC tumors ($n = 88$), normal fallopian tubes, and normal ovaries ($n = 10$ each) in TMA of patients with HGSOC, scale bars, 200 and 400 μm. **E,** Quantification of UCHL1 expression (H-score) by digital scanning of the TMA. **F,** Relative UCHL1 mRNA and protein levels in primary HGSOC tumors and matched normal adjacent fallopian tubes obtained from the same patient ($n = 9$ pairs). qPCR (top) and Western blot analysis (five pairs, bottom). **G,** Representative images of UCHL1 and p53 IHC staining and hematoxylin and eosin (H&E) staining in the serial sections of human STIC; scale bars, 400 and 200 μm. The 20× image represents a magnified section of the corresponding 10× image. **H,** Kaplan–Meier survival curves for 1,104 patients with HGSOC with low or high UCHL1 levels after chemotherapy and optimal and suboptimal debulking. Progression-free survival was analyzed by Kaplan—Meier plotter using autoselect best cutoff ($P = 0.00021$). **I,** Using OVMARK, disease-free survival of patients with HGSOC ($n = 244$) with low or high UCHL1 levels was analyzed after optimal debulking in an in-house cohort of MTCI and GSE9899 ($P = 0.004$). UCHL1 median expression was used as the cutoff. Statistical significance was determined by the log-rank test, one-way ANOVA, and Student *t* test. *, $P < 0.05$. The box boundaries represent the upper and lower quartiles, the horizontal line represents the median value, and the whiskers represent the minimum and maximum values.

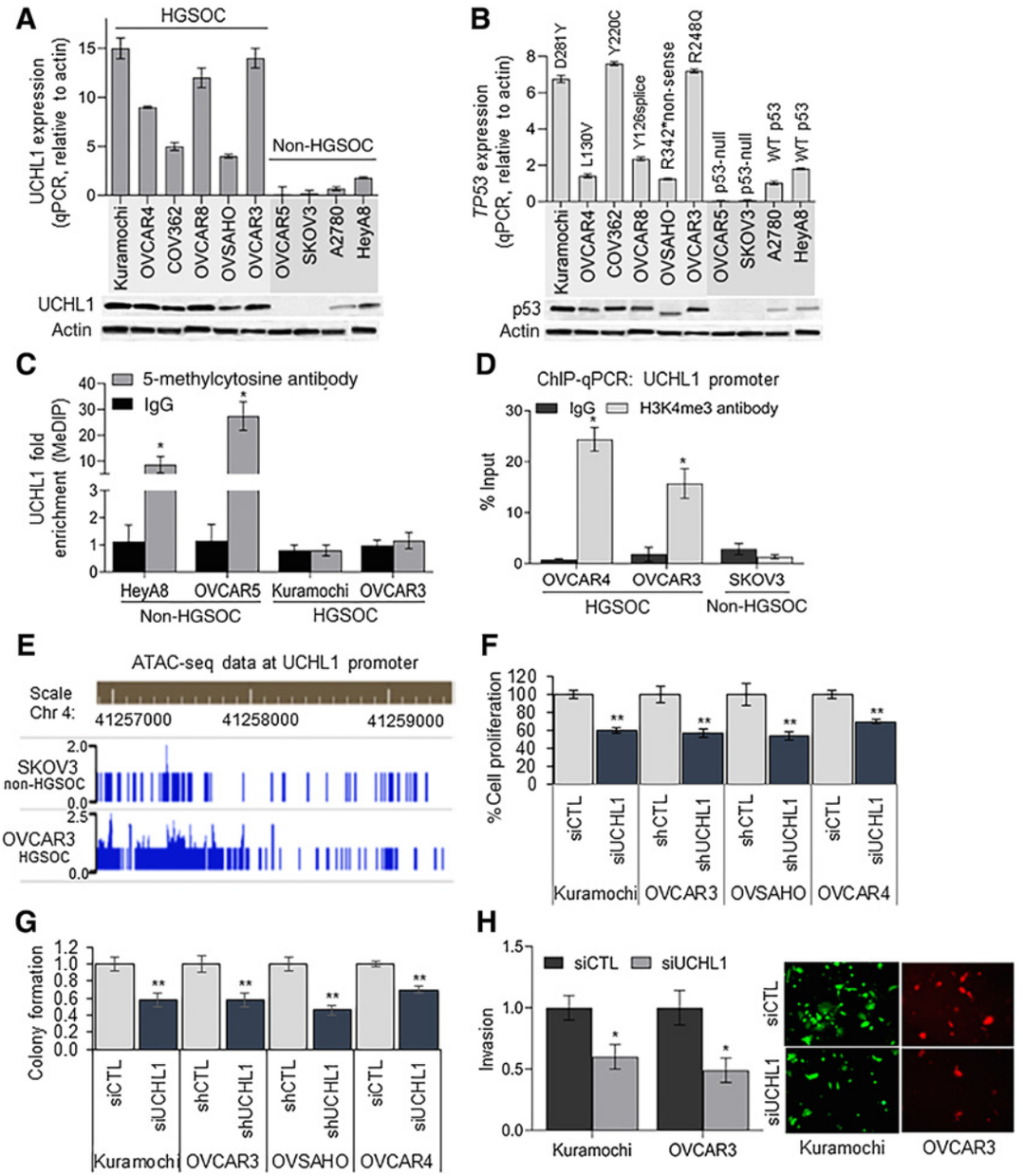

Figure 2.

Epigenetic upregulation of UCHL1 promotes HGSOC growth. **A** and **B,** UCHL1 and p53 mRNA and protein levels in HGSOC and non-HGSOC cells. Respective p53 mutation status is given above the bars showing p53 mRNA expression in **B**. UCHL1 and p53 were probed on the same blot and the same actin loading control for the blot is shown in both **A** and **B**. **C,** MeDIP was performed using 5-methylcytosine antibody or control IgG in HGSOC and non-HGSOC cells, followed by qPCR for UCHL1 promoter. Methylated DNA enrichment in the UCHL1 promoter is shown relative to control IgG. **D,** ChIP assay was performed using anti-H3K4me3 antibody or control IgG in HGSOC and non-HGSOC cells, followed by qPCR for UCHL1 promoter. H3K4me3 enrichment in the UCHL1 promoter is shown relative to the input. **E,** ATAC-seq tracks at the *UCHL1* gene loci in OVCAR3 and SKOV3 cells. Each track represents chromatin accessibility per 100 bp bin. The region shown is human chromosome 4 (chr4):41257000–41259000. **F** and **G,** Relative proliferation and clonogenic growth of HGSOC cells: Kuramochi, OVCAR3, OVCAR4, and OVSAHO, transfected with control or UCHL1 siRNA or transduced with control or UCHL1 shRNA lentiviral particles. A total of 2,000 cells per well were plated in the 96-well plates and MTT assay was performed on day 4. A total of 1,000 cells per well were plated in the 6-well plates and colonies were fixed and stained by crystal violet after 8–10 days. **H,** Invasion of OVCAR3 (RFP labeled) and Kuramochi (GFP labeled) cells transfected with control or UCHL1 siRNA through the layers of normal human omental primary mesothelial cells and fibroblasts in a transwell insert (8 μm pore size). Invaded fluorescence cells were fixed after 16 hours, imaged, and counted. Statistical significance was determined by Student *t* test from at least three independent experiments. *, $P < 0.05$; **, $P < 0.001$. See Supplementary Fig. S2. WT, wild-type.

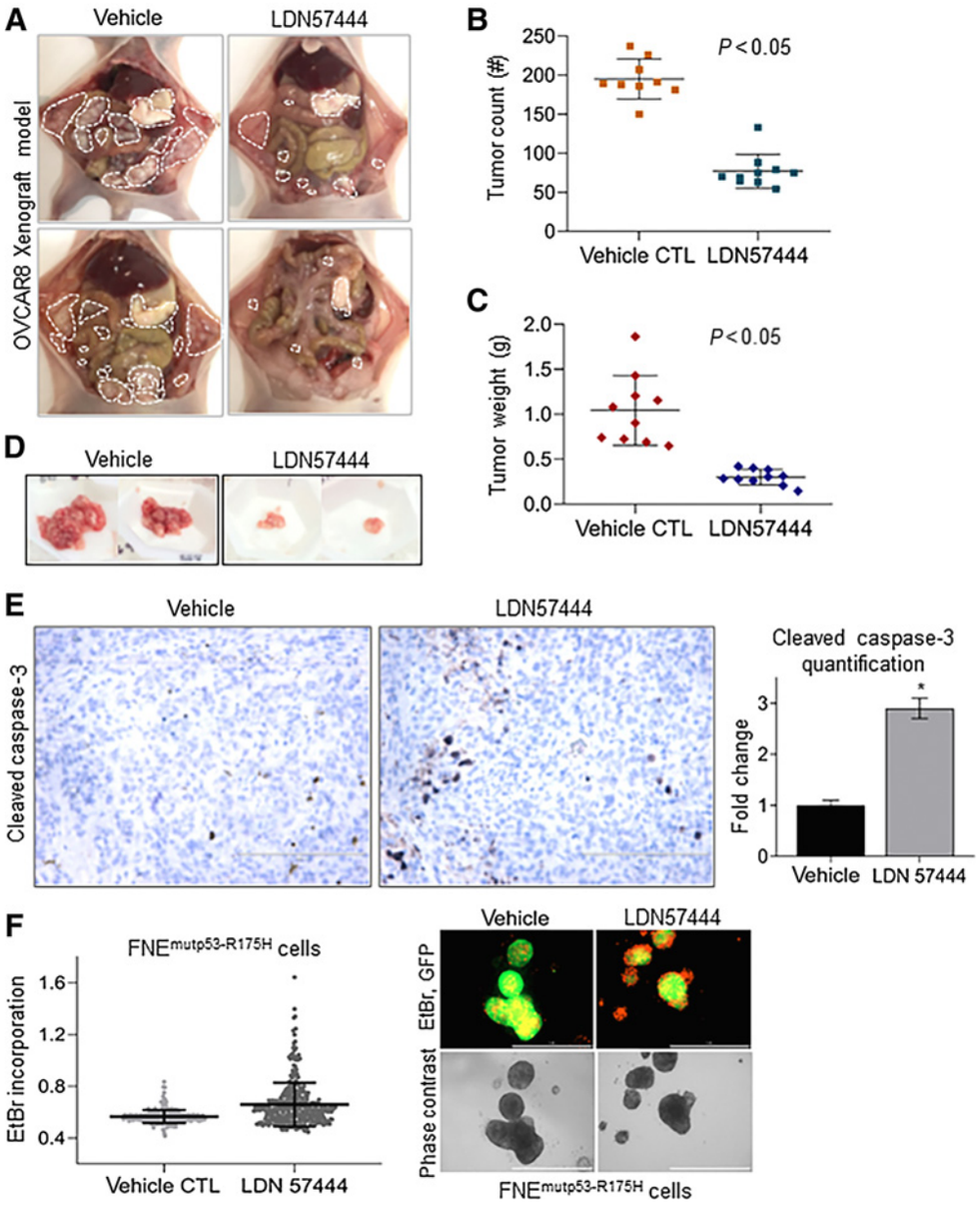

Figure 3.

Effect of UCHL1 inhibitor, LDN57444, on HGSOC metastatic growth. **A,** Female athymic nude mice were intraperitoneally injected with 5×10^6 OVCAR8 cells, and treated with vehicle control (CTL) or UCHL1 inhibitor, LDN57444, 1 mg/kg thrice per week ($n = 10$/group). Representative images of the metastatic tumor colonies outlined with the dotted white line in control and LDN57444 groups. **B,** Number of tumor nodules in the vehicle control and LDN57444-treated mice. **C,** Weight of surgically resected tumors in the vehicle control and LDN57444-treated mice. **D,** Representative images of surgically resected tumors in the vehicle control and LDN57444-treated mice. **E,** Formalin-fixed, paraffin-embedded tumor sections from control and LDN57444 groups ($n = 5$/group) were stained for cleaved caspase-3. Representative images; scale bar, 200 μm (left), and the staining quantification (right) are shown for cleaved caspase-3. **F,** FNE cells transfected with pWZL-p53-R175H were cultured in ultra-low attachment plates and treated with vehicle control or UCHL1 inhibitor, LDN57444, 10 μmol/L, for 5 days. EtBr incorporation was quantified (left) after 5 days in cellular clusters treated with DMSO ($n = 254$) or LDN57444 ($n = 334$). Representative images of DMSO- or LDN57444-treated cellular clusters of GFP-labeled $FNE^{mutp53\text{-}R175H}$ cells (right); scale bar, 1,000 μm. EtBr incorporation is visible as orange color. Data are represented as mean ± SD. Statistical significance was determined by Student *t* test (*, $P < 0.05$).

To understand the functional effects of UCHL1 in HGSOC, we knocked down UCHL1 in HGSOC cell lines: Kuramochi, OVCAR3, OVCAR4, and OVSAHO (Supplementary Fig. S2G). Cellular proliferation (**Fig. 2F**) and clonogenic growth (**Fig. 2G**; Supplementary Fig. S2H) of HGSOC cells were significantly reduced upon silencing of UCHL1. Next, we studied the effect of UCHL1 silencing on the invasion of HGSOC cells. Omentum is the most favorable site for HGSOC metastatic growth (35). To mimic the invasion of cancer cells through the outer layers of the omentum during metastasis, we utilized an organotypic 3D cell culture model of the omentum assembled in a

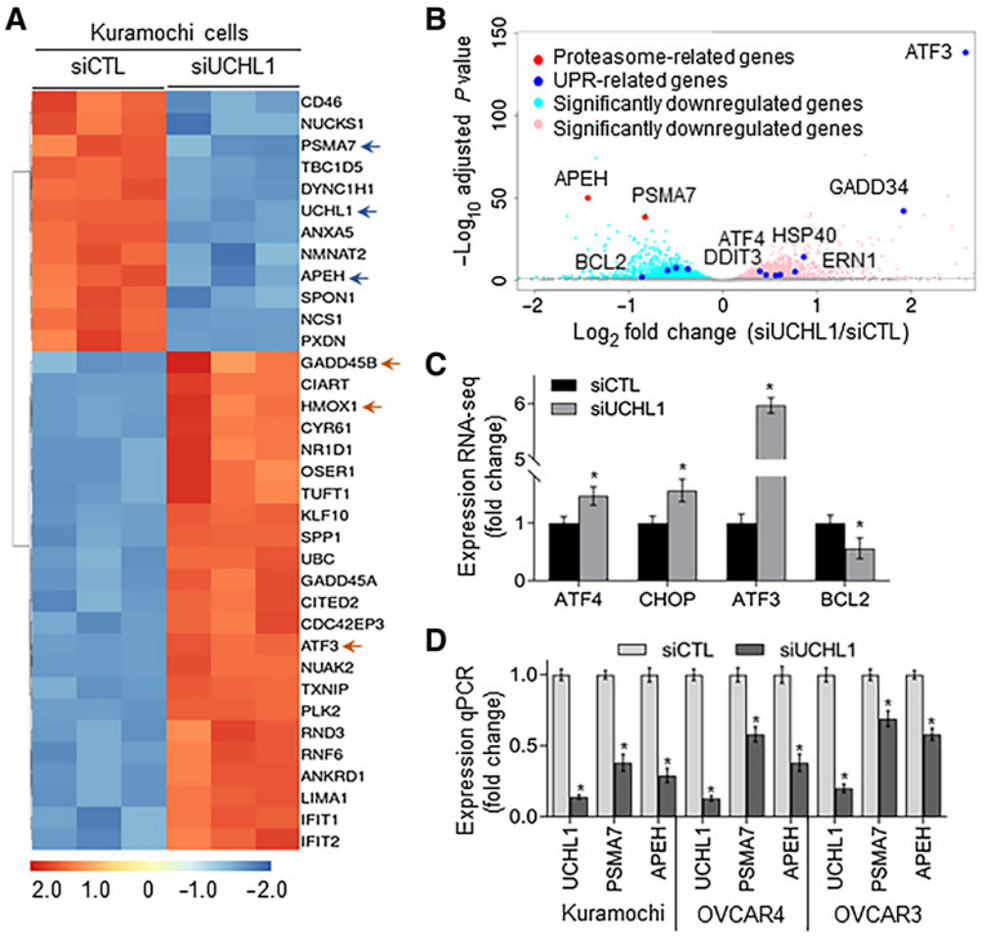

Figure 4.

UCHL1 knockdown alters the gene expression affecting proteasome function and triggering UPR. **A,** Heatmap of top 32 differentially expressed genes in the RNA-seq data of Kuramochi cells transfected with control or UCHL1 siRNA ($P < 0.005$; 1% FDR). Orange color represents upregulated genes, while the blue color represents downregulated genes. **B,** Volcano plot of significantly differentially expressed genes shows the effect of UCHL1 knockdown on the expression of UPR genes and proteasome-related genes. The *x*-axis shows the $\log_2$ fold change in the gene expression between siCTL and siUCHL1 groups, and the *y*-axis shows the *P* value for that difference. The light blue and pink dots represent downregulated and upregulated genes, respectively. The red dots represent genes implicated with proteasome activity, while the blue dots represent UPR genes. The dashed line represents $P = 0.05$ at 1% FDR. The gray dots below the dashed line represent the genes not significantly changed. **C,** Fold change in the expression of ATF4, ATF3, DDIT3 (CHOP), and Bcl2 in the RNA-seq data of Kuramochi cells transfected with control or UCHL1 siRNA. **D,** qRT-PCR validation of PSMA7 and APEH expression in Kuramochi, OVCAR4, and OVCAR3 cells transfected with control or UCHL1 siRNA.

transwell insert (ref. 35; Supplementary Fig. S2I). The invasion of UCHL1-silenced Kuramochi (GFP labeled) and OVCAR3 (RFP labeled) cells through the omental cells was significantly reduced compared with the unsilenced controls (**Fig. 2H**). Together, these data demonstrate that UCHL1 promotes growth and invasion in HGSOC.

UCHL1 inhibitor, LDN57444, inhibits HGSOC metastatic growth

To investigate the effect of UCHL1 on tumor growth *in vivo*, we treated a mouse xenograft model of HGSOC metastasis with the UCHL1 inhibitor, LDN57444. Female, athymic nude mice were intraperitoneally injected with 5×10^6 OVCAR8 cells and the peritoneal metastases were allowed to form. Subsequently, mice were intraperitoneally treated with LDN57444 (1 mg/kg) or vehicle control thrice per week (10 mice/group). Mice were euthanized 45 days after injecting the cancer cells and the tumors were counted, surgically resected, and weighed. LDN57444 treatment resulted in significantly fewer and smaller metastases compared with vehicle controls (**Fig. 3A** and **B**). Furthermore, the overall weight of the surgically resected tumors was significantly less in the LDN57444-treated mice compared with the control mice (**Fig. 3C** and **D**). Moreover, there was a marked increase in the apoptosis in the tumors treated with LDN57444 indicated by the cleaved caspase-3 staining (**Fig. 3E**). Hematoxylin and eosin staining of the tumor sections revealed that the tumors from the LDN57444 and control groups were histologically similar (Supplementary Fig. S3A). Moreover, no change in the UCHL1 expression levels was observed in the LDN57444-treated tumors compared with tumors from the control group (Supplementary Fig. S3A). Similarly, *in vitro* treatment of LDN57444, as well as UCHL1 knockdown in OVCAR8 cells significantly reduced the cell growth (Supplementary Fig. S3B–S3D). On the contrary, LDN57444 treatment in OVCAR5 cells (with no endogenous UCHL1 expression) showed no effect on the cellular proliferation (Supplementary Fig. S3E), demonstrating the specificity of LDN57444 for UCHL1. These results demonstrate the

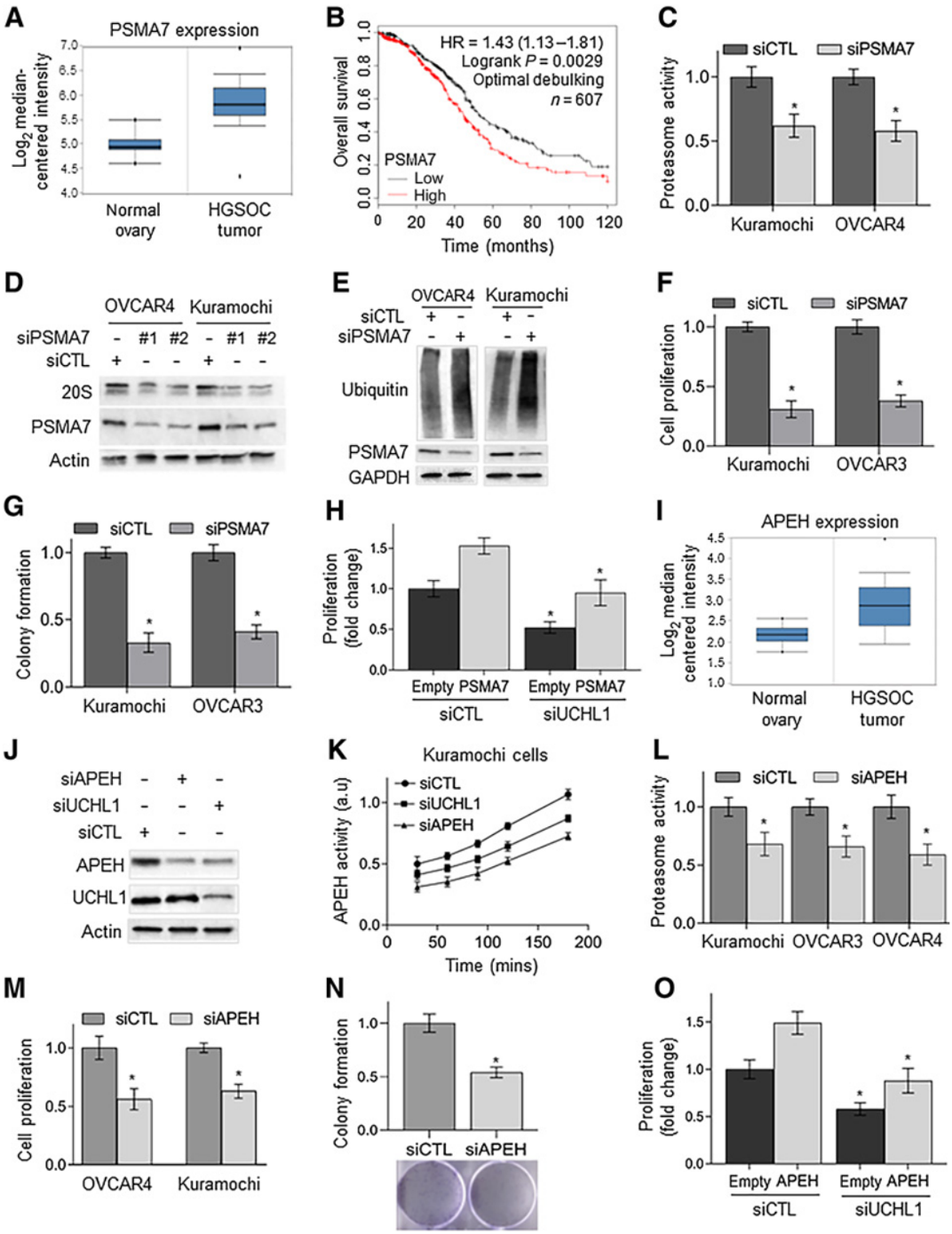

Figure 5.

PSMA7 and APEH mediate proteasome activity and HGSOC growth. **A,** PSMA7 mRNA expression in normal ovary and HGSOC patient tumors in TCGA database analyzed using Oncomine gene browser. **B,** Kaplan–Meier survival curves showing overall survival of 607 patients with HGSOC with low or high PSMA7 levels after optimal debulking and chemotherapy analyzed by Kaplan—Meier plotter ($P = 0.0027$). **C,** Chymotrypsin-like proteasome activity was measured using fluorescence substrate, LLVY-R110, in cell lysates of OVCAR4 and Kuramochi cells transfected with control or PSMA7 siRNA. The cleavage of LLVY-R110 by proteasomes was monitored fluorometrically. **D** and **E,** Representative immunoblot analysis of 20S proteasome, PSMA7, and total ubiquitinated proteins in the whole-cell lysate of OVCAR4 and Kuramochi cells transfected with control or PSMA7 siRNA. **F** and **G,** The relative proliferation and clonogenic growth of HGSOC cells transfected with control or PSMA7 siRNA. A total of 2,000 cells per well were plated in the 96-well plates and MTT assay was performed on day 4. A total of 1,000 cells per well were plated in the 6-well plates and colonies were fixed and stained by crystal violet after 8–10 days. **H,** The relative proliferation of UCHL1-silenced OVCAR4 cells after PSMA7 overexpression. (*Continued on the following page.*)

potential of inhibiting UCHL1 to abrogate the metastatic growth *in vivo*.

HGSOC precursor lesions in the fallopian tube uniquely disseminate through the peritoneal fluid, largely depending on the anchorage-independent survival of cancer cells. Therefore, we next studied the effect of UCHL1 inhibitor, LDN57444, on anchorage-independent survival using a model of such early dissemination consisting of spheroids of FNE cells transfected with pWZL-p53-R175H ($FNE^{mutp53\text{-}R175H}$). Compared with empty vector controls, prolonged anchorage-independent survival of $FNE^{mutp53\text{-}R175H}$ spheroids, overexpressing mutant p53 variant R175, has been reported previously (34). We observed increased expression of UCHL1 in $FNE^{mutp53\text{-}R175H}$ cells (Supplementary Fig. S3F). The cell death of $FNE^{mutp53\text{-}R175H}$ spheroids was significantly increased upon LDN57444 (10 μmol/L, 5 days) treatment (**Fig. 3F**). Increased EtBr intercalation into DNA due to cell death associated with nuclear membrane fracture and reduced GFP expression was observed in the LDN57444-treated $FNE^{mutp53\text{-}R175H}$ spheroids compared with control spheroids (**Fig. 3F**). These results indicate that UCHL1 inhibition affects the growth of $FNE^{mutp53\text{-}R175H}$ spheroids. Collectively, the data demonstrate that UCHL1 affects HGSOC metastatic growth.

UCHL1 knockdown results in upregulation of UPR genes and downregulation of genes implicated with proteasome activity

UCHL1 is known for its varied functions, including DNA binding, translation initiation, and influencing gene expression (46–48). To understand the global effect of UCHL1 knockdown in HGSOC, we conducted an RNA-seq analysis in the UCHL1-silenced Kuramochi cells. A total of 1,004 genes were differentially expressed in Kuramochi cells upon silencing of UCHL1 ($P < 0.05$ and FDR = 1%). Analysis of the top 35 dysregulated genes (**Fig. 4A**) revealed the upregulation of stress-induced genes, including *heme oxygenase 1* (*HMOX1*), a heat-shock factor 1 (HSF1) target gene (16); *growth arrest and DNA damage inducible, beta* (*GADD45b*); and *activating transcription factor 3* (*ATF3*), an ER stress–induced gene. Further analysis of the differentially expressed genes revealed upregulation of UPR genes *DDIT3* (*CHOP*), *ATF4, ATF3, GADD35*, and *HSP40* in UCHL1-silenced Kuramochi cells (**Fig. 4B** and **C**). In contrast, the expression of PSMA7 and APEH, implicated with proteasome or proteasome activity, was downregulated in our RNA-seq data (**Fig. 4A** and **B**) and subsequently qRT-PCR validated in UCHL1-silenced HGSOC cells (**Fig. 4D**). Inhibition of proteasome activity has been associated with the induction of terminal UPR (9, 49). These results indicate the plausible role of UCHL1 in mediating protein degradation and ER stress in HGSOC.

PSMA7 and APEH mediate proteasome activity and HGSOC growth

We next studied the functional role of PSMA7 and APEH, the two potential downstream effectors of UCHL1 identified in our RNA-seq data of UCHL1-silenced Kuramochi cells. PSMA7-associated alternative proteasome isoform has been reported to exhibit enhanced resistance to stress in yeast and primed mammalian cells (50). However, not much is known about the role of PSMA7 in rendering cancer cells resistant to proteotoxic stress. To evaluate the clinical significance of PSMA7 in HGSOC, we analyzed the expression of PSMA7 in HGSOC patient tumors in TCGA database. PSMA7 expression was high in HGSOC tumors (**Fig. 5A**) and correlated with poor overall survival of patients with HGSOC after optimal debulking (**Fig. 5B**). Moreover, a positive and significant correlation ($r = 0.3$; $P = 1.93e\text{-}9$) was observed between UCHL1 and PSMA7 in HGSOC patient tumors (Supplementary Fig. S4A). Silencing of PSMA7 resulted in significantly reduced chymotrypsin-like proteasome activity and 20S proteasome levels in HGSOC cells (**Fig. 5C** and **D**), leading to the accumulation of polyubiquitinated proteins (**Fig. 5E**). Consistent with these findings, cellular proliferation and clonogenic growth of HGSOC cells were significantly reduced upon silencing of PSMA7 (**Fig. 5F** and **G**). These results suggest that PSMA7-mediated proteasome activity is required for HGSOC growth. To further examine the link between UCHL1 and PSMA7, we overexpressed PSMA7 in UCHL1-silenced cells (Supplementary Fig. S4B). PSMA7 overexpression rescued the effect of UCHL1 silencing on the cellular proliferation of OVCAR4 cells (**Fig. 5H**), suggesting that PSMA7 acts as a functional effector of UCHL1 in HGSOC. However, silencing of PSMA7 did not alter the expression of UCHL1 (Supplementary Fig. S4C), indicating the absence of feedback regulation. Collectively, the data demonstrate that UCHL1 and PSMA7 support HGSOC growth through sustained proteasomal activity and degradation.

The activity of the cytosolic enzyme, APEH, has been reported to be associated with increased proteasome activity (37). APEH catalyzes the removal of *N*-acetylated amino acid from the acetylated peptides, releasing the free amino acids. The activity of APEH possibly disrupts the negative feedback inhibition of proteasomal activity caused by the accumulation of *N*-acetylated peptides after proteasomal degradation of proteins (37). In TCGA database, the expression of APEH was significantly higher in HGSOC tumors compared with normal ovaries (**Fig. 5I**). Silencing of UCHL1 or APEH resulted in reduced APEH expression, leading to a decrease in APEH activity in HGSOC cells (**Fig. 5J** and **K**; Supplementary Fig. S4D). Silencing of APEH also resulted in significantly reduced chymotrypsin-like proteasome activity in HGSOC cells (**Fig. 5L**). These results suggest that UCHL1 regulates APEH activity through altering its expression, which in turn regulates proteasome activity. Consistent with these results, cellular proliferation and clonogenic growth of HGSOC cells were significantly reduced upon silencing of APEH (**Fig. 5M** and **N**). Moreover, APEH overexpression in UCHL1-silenced cells rescued the effect of UCHL1 silencing on the cellular proliferation of OVCAR4 cells (**Fig. 5O**; Supplementary Fig. S4E). These results suggest that

(*Continued.*) OVCAR4 cells were cotransfected with control (siCTL) or UCHL1 (siUCHL1) siRNA and PSMA7 or empty vector. The MTT assay was performed on day 5. **I,** APEH mRNA expression in normal ovary and HGSOC patient tumors in TCGA database analyzed using Oncomine gene browser. **J,** Representative immunoblot analysis of APEH and UCHL1 in the whole-cell lysate of Kuramochi cells transfected with control or UCHL1 or APEH siRNA. **K,** APEH activity was measured by acetyl-Ala-*p*-nitroanilide in the total cell lysate of HGSOC cells transfected with control or UCHL1 or APEH siRNA. The cleavage of colorimetric p-nitroanilide by APEH was measured at different timepoints. **L,** Chymotrypsin-like proteasome activity was measured using fluorescence substrate, LLVY-R110, in OVCAR3, OVCAR4, and Kuramochi cells transfected with control or APEH siRNA. The cleavage of LLVY-R110 by proteasomes was monitored fluorometrically. **M** and **N,** The relative proliferation and clonogenic growth of Kuramochi and OVCAR4 cells transfected with control or APEH siRNA. A total of 2,000 cells per well were plated in the 96-well plates and MTT assay was performed on day 4. A total of 1,000 cells per well were plated in the 6-well plates and colonies were fixed and stained by crystal violet after 8–10 days. **O,** The relative proliferation of UCHL1-silenced OVCAR4 cells after APEH overexpression. OVCAR4 cells were cotransfected with control or UCHL1 siRNA and APEH or empty vector. The MTT assay was performed on day 5. Statistical significance was determined by unpaired Student *t* test from at least three independent experimental repeats, *, $P < 0.05$. The box boundaries represent the upper and lower quartiles, the horizontal line represents the median value, and the whiskers represent the minimum and maximum values.

APEH is a downstream effector of UCHL1 and its expression and enzymatic activity affect proteasome activity and HGSOC growth. Next, we studied the relationship between APEH and PSMA7, APEH expression was significantly reduced upon silencing of PSMA7 (Supplementary Fig. S4C). Supporting these results, a positive correlation ($r = 0.2$; $P = 6.22e\text{-}4$) was observed between APEH and PSMA7 in HGSOC patient tumors in TCGA data. Collectively, these results demonstrate that UCHL1 mediates proteasome activity and HGSOC growth through PSMA7 and APEH. The exact mechanism by which UCHL1 regulates PSMA7 and APEH expression needs to be further investigated.

UCHL1 inhibition attenuates mTORC1 activity and induces a terminal stress response

Inhibition of proteasomal degradation of unfolded, misfolded, and damaged proteins results in proteotoxicity, leading to activation of terminal UPR and attenuation of protein translation (9, 51, 52). We hypothesized that UCHL1 inhibition potentially renders HGSOC cells vulnerable to proteotoxicity through impaired proteasomal activity and degradation of proteins. UCHL1 knockdown, and treatment with UCHL1 inhibitor, LDN57444, resulted in the accumulation of polyubiquitinated proteins in HGSOC cells, Kuramochi and OVCAR4 (**Fig. 6A** and **B**). Moreover, proteasome activity was significantly reduced in LDN57444-treated xenograft tumors (**Fig. 6C**). Consistent with these results, UCHL1 inhibition resulted in increased levels of phospho-EIF2α, ATF4, ATF3, CHOP, and cleaved caspase-3, while the expression of antiapoptotic protein, BCL2, was decreased (**Fig. 6D** and **E**). Together with our RNA-seq data (**Fig. 4B** and **C**), these results suggest that activation of PERK/ATF4/ATF3/CHOP promotes cell death in UCHL1-silenced cells. To further confirm these results, we cosilenced EIF2AK3 (PERK) and UCHL1 in Kuramochi cells. Increased DDIT3 (CHOP) expression in the UCHL1-silenced cells was significantly reduced upon cosilencing EIF2AK3 and UCHL1 (**Fig. 6F**). Consistent with these findings, mTORC1 activity and protein synthesis were significantly reduced in UCHL1-silenced cells, evidenced by decreased phosphorylated levels of two mTORC1 substrates, ribosomal protein S6 (S6) and the eukaryotic initiation factor 4E-binding protein (4EBP1; **Fig. 6D** and **E**). Collectively, the data demonstrate that UCHL1 inhibition results in impaired proteasomal degradation and accumulation of polyubiquitinated proteins, leading to attenuation of protein synthesis and activation of terminal UPR (**Fig. 6G**). Overall, the data demonstrate that UCHL1 maintains protein homeostasis and promotes HGSOC growth by mediating proteasomal degradation of ubiquitinated proteins through the PSMA7–APEH–proteasome axis.

Discussion

DUBs have been implicated in regulating many processes associated with tumor progression and are emerging as prognostic markers due to their correlation with tumor grade and stage (21, 53, 54). UCHL1 is a cancer-associated DUB, reported as either an overexpressed oncogene (21–23, 55) or an epigenetically silenced tumor suppressor (25, 26, 56) in several malignancies. Previous studies have reported the role of UCHL1 in promoting metastasis by its deubiquitinating activity associated with HIF1α, cyclin B1, and TGFβ receptor 1 (21, 22, 24). This study demonstrates that UCHL1 overexpression in HGSOC patient tumors correlates with tumor grade and stage and predicts poor prognosis. We showed that UCHL1 promotes HGSOC growth by mediating protein homeostasis through the PSMA7–APEH–proteasome axis. Inhibiting UCHL1 increases ER stress and induces terminal UPR because of impaired proteasome activity and accumulation of polyubiquitinated proteins in HGSOC cells. Previous studies have reported the induction of proteotoxic stress and cancer cell death by broadly inhibiting DUBs using a pan-DUB inhibitor and inhibitor of proteasome-associated DUBs (16, 57). Our study identifies a specific DUB that mediates protein homeostasis, potentially through its association with the proteasome or cooperation with the UPR-mediated prosurvival signaling. Moreover, about 96% of patients with HGSOC harbor *TP53* mutations. Previous studies have reported the role of the mutant p53–NRF2 axis and mutant p53–HSF1 axis in the transcriptional upregulation of proteasomal machinery (36) and rendering cancer cells more resistant to the proteotoxic and ER stress (58, 59). Our patient data showed a weak correlation ($r = 0.2$) between UCHL1 and mutant p53 expression levels in patients with HGSOC with missense *TP53* mutations. Increased UCHL1 expression was also observed in STICs, and HGSOC cell lines harboring *TP53* mutations. Together, these findings indicate the context-dependent upregulation of UCHL1 in HGSOC and a potential link between mutant p53 and UCHL1. Further studies are required to delineate the role of gain-of-function p53 mutation in regulating UCHL1 expression. HGSOC originates from the fallopian tube secretory epithelial cells (FTSEC; ref. 51). FTSECs are characterized by abundant rough ER and well-developed Golgi complexes with secretory vesicles, a feature that remains maintained in the malignant state (51), indicating that these cancer cells are primed for high protein synthesis, which makes them dependent on the protein quality control pathways to maintain protein homeostasis (51). From a translational perspective, this indicates the HGSOC vulnerability to imbalances in protein homeostasis, and our study identifies novel links in this proteostasis network.

UCHL1 is mainly a neuronal DUB, and it constitutes about 1%–2% of total brain proteins. The loss of UCHL1 has been implicated in neurodegenerative diseases, resulting in the accumulation of neuronal protein aggregates because of impaired proteasomal degradation (19, 20). However, the exact mechanism by which UCHL1 regulates proteasome activity remains elusive. For the first time, we report that increased expression of PSMA7 and APEH in HGSOC regulates proteasome activity and their association with the UCHL1-mediated proteostasis. Upregulation of proteasome subunits (PSMA3, PSMB5, and PSMA7) or proteasome assembly factors promotes resistance to ER stress and proteasome inhibitors in cancer (12, 50, 60, 61). Specifically, the evolutionarily conserved PSMA7 proteasome isoform has been shown to provide tolerance to oxidative stress in the mammalian cells primed to form PSMA7 proteasome isoform (50). Similarly, APEH regulates proteasome activity potentially by disrupting the negative feedback inhibition of proteasomal activity caused by the accumulation of acetylated peptides (37). Our findings revealed a correlation between APEH and PSMA7 expression in patient's tumors and their role in maintaining protein homeostasis through increased proteasomal activity and protein degradation. Our alternative approach of determining genes and pathways transcriptionally deregulated by UCHL1 knockdown identified PSMA7 and APEH as the key downstream effectors of UCHL1. UCHL1 is known for its varied functions, including interaction with DNA, gene transcription, and translation initiation (46–48). It could be involved in a direct mechanism regulating transcription of these genes or through a mechanism involving UPR and regulation of proteostasis. Further studies are needed to identify the mechanism of their transcriptional regulation and the role of UCHL1 in this process.

UCHL1 has been reported as an epigenetically silenced tumor suppressor in several malignancies. A previous study (26) has reported UCHL1 as an epigenetically silenced gene in ovarian cancer; however,

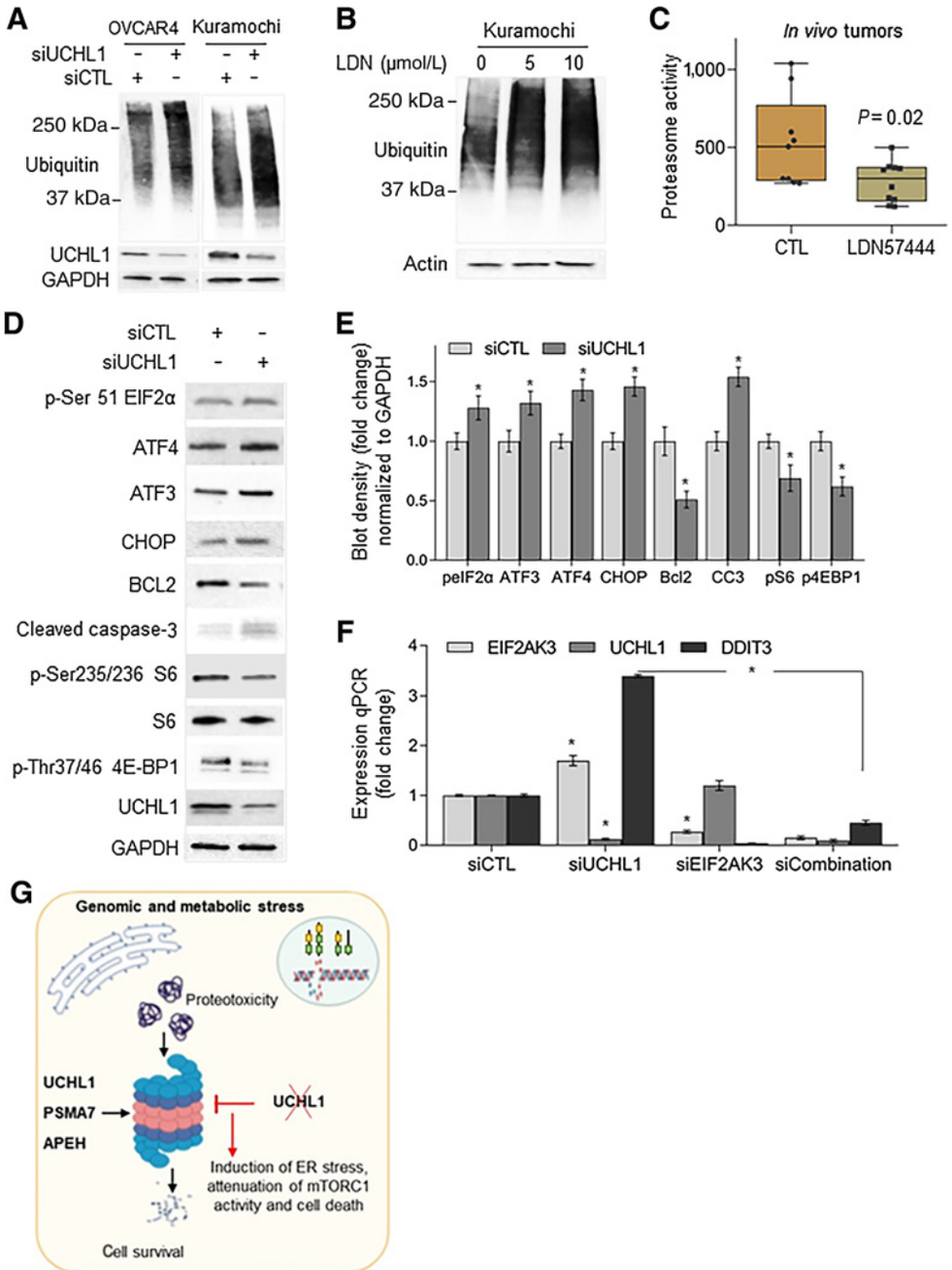

Figure 6.

UCHL1 inhibition attenuates mTORC1 activity and induces a terminal ER stress response. **A,** Representative immunoblot analysis of total ubiquitinated proteins in OVCAR4 and Kuramochi HGSOC cells transfected with control (CTL) or UCHL1 siRNA. **B,** Representative immunoblot analysis of total ubiquitinated proteins in Kuramochi cells treated with vehicle control or UCHL1 inhibitor, LDN57444 (5 and 10 μmol/L) for 24 hours. **C,** Chymotrypsin-like proteasome activity was measured using substrate LLVY-R110 in the tissue homogenate of OVCAR8 xenograft tumors treated with the vehicle control or UCHL1 inhibitor, LDN57444. The cleavage of LLVY-R110 by proteasomes was monitored fluorometrically. **D** and **E,** Representative immunoblot analysis of target proteins in Kuramochi cells transfected with control or UCHL1 siRNA. The blot density for each protein was quantified and normalized to the density of GAPDH. The data are presented as a fold change compared with siCTL. **F,** Kuramochi cells were transfected with control or UCHL1 or EIF2AK3 (PERK) or UCHL1 + EIF2AK3 (siCombination) siRNA. The expression of UCHL1, EIF2AK3, and DDIT3 (CHOP) was assessed by qRT-PCR. **G,** Schematic showing the role of the UCHL1–PSMA7–APEH–proteasome axis in mediating protein homeostasis and HGSOC cell survival. UCHL1 inhibition results in impaired proteasome activity and protein degradation resulting in the accumulation of polyubiquitinated proteins, reduced mTORC1 activity and translation, and induction of UPR-mediated cell death. Statistical significance was determined by unpaired Student *t* test from at least three independent experimental repeats, *, $P < 0.05$. The box boundaries represent the upper and lower quartiles, the horizontal line represents the median value, and the whiskers represent the minimum and maximum values.

UCHL1 was methylated in only one of 17 tumors they studied (26). Furthermore, the information on the ovarian cancer histotype was not provided (26). Our findings revealed consistent upregulation of UCHL1 in multiple HGSOC datasets, including TCGA. Furthermore, TCGA methylation data analysis showed hypomethylation at *UCHL1* gene loci in serous ovarian cancer tumors, corroborating with our MeDIP, ChIP, and ATAC-seq data in HGSOC cells. Our findings revealed hypomethylation at the UCHL1 promoter and epigenetic upregulation of UCHL1 in HGSOC. Mutant p53 has been shown to transcriptionally upregulate the expression of H3K4 histone methyltransferases in breast cancer (33), which in turn governs open chromatin and hypomethylation at gene loci. Together, this suggests a potential mechanism of UCHL1 induction in HGSOC through mutant p53.

Targeting protein homeostasis by directly inhibiting proteasome activity has been clinically successful in certain tumor types, such as multiple myeloma, possibly owing to its dependence on protein quality control pathways due to the inherently high protein synthesis rate (7). Furthermore, in solid tumors, such as lung, pancreas, and head and neck cancer, the second-generation proteasome inhibitor, carfilzomib, has started to show better results due to greater selectivity, inhibitory potency for proteasome subunits, and an improved clinical safety profile than bortezomib (7). These reports suggest that targeting DUBs to induce proteotoxic stress is a viable approach to treat solid tumors (16, 57). Various small-molecule DUB inhibitors are emerging as therapeutic modalities for cancer treatment, such as the USP14 inhibitor, VLX1570 in myeloma, NCT02372240 (62). Our study identified the role of UCHL1 in mediating protein homeostasis in HGSOC and the potential of inhibiting UCHL1 and APEH to sensitize cancer cells to proteotoxic stress in solid tumors.

Authors' Disclosures

R. Drapkin reports personal fees from Repare Therapeutics, VOC Health, and Siamab Therapeutics outside the submitted work. S. Mitra reports a patent for 16/774,460 pending. No disclosures were reported by the other authors.

Authors' Contributions

A. Tangri: Validation, investigation. **K. Lighty:** Validation, investigation. **J. Loganathan:** Validation, investigation. **F. Mesmar:** Validation, methodology. **R. Podicheti:** Formal analysis. **C. Zhang:** Formal analysis. **M. Iwanicki:** Investigation, methodology. **R. Drapkin:** Resources, validation. **H. Nakshatri:** Resources, writing–review and editing. **S. Mitra:** Conceptualization, resources, supervision, funding acquisition, investigation, methodology, writing–original draft, project administration, writing–review and editing.

Acknowledgments

This research was funded by Ovarian Cancer Research Alliance (grant no. 544389 to S. Mitra). This work was also supported by the pilot grants from the Ralph W. and Grace M. Showalter Trust and a Biomedical Research grant from Indiana University School of Medicine (to S. Mitra). The authors are thankful to Dr. George Sandusky and Ms. Constance J Temm, Department of Pathology, IU Health, for their help in tissue microarray analysis and IHC. We are thankful to Dr. Anirban Mitra, IU Bloomington for his help in the xenograft experiment and 3D omental culture. We thank Dr. Yunlong Liu, Dr. Yue Wang, and Ms. Xiaona Chu, Center for Medical Genomics for ATAC-seq. We also thank Douglas B. Rusch, Center for Genomics and Bioinformatics. The authors are thankful to Indiana University Simon Comprehensive Cancer Center for their support and help in tissue procurement.

The costs of publication of this article were defrayed in part by the payment of page charges. This article must therefore be hereby marked *advertisement* in accordance with 18 U.S.C. Section 1734 solely to indicate this fact.

Received October 9, 2020; revised February 10, 2021; accepted March 17, 2021; published first March 22, 2021.

References

1. Schubert U, Antón LC, Gibbs J, Norbury CC, Yewdell JW, Bennink JR. Rapid degradation of a large fraction of newly synthesized proteins by proteasomes. Nature 2000;404:770–4.
2. Guang MHZ, Kavanagh EL, Dunne LP, Dowling P, Zhang L, Lindsay S, et al. Targeting proteotoxic stress in cancer: a review of the role that protein quality control pathways play in oncogenesis. Cancers 2019;11:66.
3. Mantovani F, Collavin L, Del Sal G. Mutant p53 as a guardian of the cancer cell. Cell Death Differ 2019;26:199–212.
4. Donnelly N, Storchová Z. Aneuploidy and proteotoxic stress in cancer. Mol Cell Oncol 2015;2:e976491.
5. Bastola P, Oien DB, Cooley M, Chien J. Emerging cancer therapeutic targets in protein homeostasis. AAPS J 2018;20:94.
6. Reeg S, Jung T, Castro JP, Davies KJA, Henze A, Grune T. The molecular chaperone Hsp70 promotes the proteolytic removal of oxidatively damaged proteins by the proteasome. Free Radic Biol Med 2016;99:153–66.
7. Roeten MSF, Cloos J, Jansen G. Positioning of proteasome inhibitors in therapy of solid malignancies. Cancer Chemother Pharmacol 2018;81:227–43.
8. Naujokat C, Hoffmann S. Role and function of the 26S proteasome in proliferation and apoptosis. Lab Invest 2002;82:965–80.
9. Obeng EA, Carlson LM, Gutman DM, Harrington WJ, Lee KP, Boise LH. Proteasome inhibitors induce a terminal unfolded protein response in multiple myeloma cells. Blood 2006;107:4907–16.
10. Pakos-Zebrucka K, Koryga I, Mnich K, Ljujic M, Samali A, Gorman AM. The integrated stress response. EMBO Rep 2016;17:1374–95.
11. Suraweera A, Münch C, Hanssum A, Bertolotti A. Failure of amino acid homeostasis causes cell death following proteasome inhibition. Mol Cell 2012;48:242–53.
12. Xu H, Han H, Song S, Yi N, Qian C, Qiu Y, et al. Exosome-transmitted PSMA3 and PSMA3-AS1 promote proteasome inhibitor resistance in multiple myeloma. Clin Cancer Res 2019;25:1923–35.
13. Ali A, Wang Z, Fu J, Ji L, Liu J, Li L, et al. Differential regulation of the REGgamma-proteasome pathway by p53/TGF-beta signalling and mutant p53 in cancer cells. Nat Commun 2013;4:2667.
14. Chondrogianni N, Tzavelas C, Pemberton AJ, Nezis IP, Rivett AJ, Gonos ES. Overexpression of proteasome beta5 assembled subunit increases the amount of proteasome and confers ameliorated response to oxidative stress and higher survival rates. J Biol Chem 2005;280:11840–50.
15. Zhang X, Schulz R, Edmunds S, Krüger E, Markert E, Gaedcke J, et al. MicroRNA-101 suppresses tumor cell proliferation by acting as an endogenous proteasome inhibitor via targeting the proteasome assembly factor POMP. Mol Cell 2015;59:243–57.
16. Harris IS, Endress JE, Coloff JL, Selfors LM, McBrayer SK, Rosenbluth JM, et al. Deubiquitinases maintain protein homeostasis and survival of cancer cells upon glutathione depletion. Cell Metab 2019;29:1166–81.
17. Mofers A, Pellegrini P, Linder S, D'Arcy P. Proteasome-associated deubiquitinases and cancer. Cancer Metastasis Rev 2017;36:635–53.
18. Setsuie R, Wada K. The functions of UCH-L1 and its relation to neurodegenerative diseases. Neurochem Int 2007;51:105–11.
19. Lombardino AJ, Li X-C, Hertel M, Nottebohm F. Replaceable neurons and neurodegenerative disease share depressed UCHL1 levels. Proc Natl Acad Sci U S A 2005;102:8036–41.
20. Graham SH, Liu H. Life and death in the trash heap: the ubiquitin proteasome pathway and UCHL1 in brain aging, neurodegenerative disease and cerebral Ischemia. Ageing Res Rev 2017;34:30–8.
21. Goto Y, Zeng L, Yeom CJ, Zhu Y, Morinibu A, Shinomiya K, et al. UCHL1 provides diagnostic and antimetastatic strategies due to its deubiquitinating effect on HIF-1alpha. Nat Commun 2015;6:6153.
22. Kwan SY, Au-Yeung CL, Yeung TL, Rynne-Vidal A, Wong KK, Risinger JI, et al. Ubiquitin carboxyl-terminal hydrolase L1 (UCHL1) promotes uterine serous cancer cell proliferation and cell cycle progression. Cancers 2020;12:118.

23. Hussain S, Bedekovics T, Chesi M, Bergsagel PL, Galardy PJ. UCHL1 is a biomarker of aggressive multiple myeloma required for disease progression. Oncotarget 2015;6:40704–18.
24. Liu S, González-Prieto R, Zhang M, Geurink PP, Kooij R, Iyengar PV, et al. Deubiquitinase activity profiling identifies UCHL1 as a candidate oncoprotein that promotes TGFβ-induced breast cancer metastasis. Clin Cancer Res 2020;26: 1460–73.
25. Ummanni R, Jost E, Braig M, Lohmann F, Mundt F, Barett C, et al. Ubiquitin carboxyl-terminal hydrolase 1 (UCHL1) is a potential tumour suppressor in prostate cancer and is frequently silenced by promoter methylation. Mol Cancer 2011;10:129.
26. Okochi-Takada E, Nakazawa K, Wakabayashi M, Mori A, Ichimura S, Yasugi T, et al. Silencing of the UCHL1 gene in human colorectal and ovarian cancers. Int J Cancer 2006;119:1338–44.
27. Bowtell DD, Böhm S, Ahmed AA, Aspuria P-J, Bast RC, Beral V, et al. Rethinking ovarian cancer II: reducing mortality from high-grade serous ovarian cancer. Nat Rev Cancer 2015;15:668–79.
28. Rhodes DR, Yu J, Shanker K, Deshpande N, Varambally R, Ghosh D, et al. ONCOMINE: a cancer microarray database and integrated data-mining platform. Neoplasia 2004;6:1–6.
29. Gyorffy B, Lanczky A, Szallasi Z. Implementing an online tool for genome-wide validation of survival-associated biomarkers in ovarian-cancer using microarray data from 1287 patients. Endocr Relat Cancer 2012;19:197–208.
30. Madden SF, Clarke C, Stordal B, Carey MS, Broaddus R, Gallagher WM, et al. OvMark: a user-friendly system for the identification of prognostic biomarkers in publicly available ovarian cancer gene expression datasets. Mol Cancer 2014; 13:241.
31. Gao J, Aksoy BA, Dogrusoz U, Dresdner G, Gross B, Sumer SO, et al. Integrative analysis of complex cancer genomics and clinical profiles using the cBioPortal. Sci Signal 2013;6:pl1.
32. Ladanyi A, Mukherjee A, Kenny HA, Johnson A, Mitra AK, Sundaresan S, et al. Adipocyte-induced CD36 expression drives ovarian cancer progression and metastasis. Oncogene 2018;37:2285–301.
33. Zhu J, Sammons MA, Donahue G, Dou Z, Vedadi M, Getlik M, et al. Gain-of-function p53 mutants co-opt chromatin pathways to drive cancer growth. Nature 2015;525:206–11.
34. Iwanicki MP, Chen HY, Iavarone C, Zervantonakis IK, Muranen T, Novak M, et al. Mutant p53 regulates ovarian cancer transformed phenotypes through autocrine matrix deposition. JCI Insight 2016;1:e86829.
35. Tomar S, Plotnik JP, Haley J, Scantland J, Dasari S, Sheikh Z, et al. ETS1 induction by the microenvironment promotes ovarian cancer metastasis through focal adhesion kinase. Cancer Lett 2018;414:190–204.
36. Walerych D, Lisek K, Sommaggio R, Piazza S, Ciani Y, Dalla E, et al. Proteasome machinery is instrumental in a common gain-of-function program of the p53 missense mutants in cancer. Nat Cell Biol 2016;18:897–909.
37. Palumbo R, Gogliettino M, Cocca E, Iannitti R, Sandomenico A, Ruvo M, et al. APEH inhibition affects osteosarcoma cell viability via downregulation of the proteasome. Int J Mol Sci 2016;17:1614.
38. Singh KP, Treas J, Tyagi T, Gao W. DNA demethylation by 5-aza-2-deoxycytidine treatment abrogates 17 beta-estradiol-induced cell growth and restores expression of DNA repair genes in human breast cancer cells. Cancer Lett 2012; 316:62–9.
39. Langmead B, Salzberg SL. Fast gapped-read alignment with Bowtie 2. Nat Methods 2012;9:357–9.
40. Consortium EP. An integrated encyclopedia of DNA elements in the human genome. Nature 2012;489:57–74.
41. Kent WJ, Sugnet CW, Furey TS, Roskin KM, Pringle TH, Zahler AM, et al. The human genome browser at UCSC. Genome Res 2002;12:996–1006.
42. Anders S, Pyl PT, Huber W. HTSeq–a Python framework to work with high-throughput sequencing data. Bioinformatics 2015;31:166–9.
43. Mitra S, Tiwari K, Podicheti R, Pandhiri T, Rusch DB, Bonetto A, et al. Transcriptome profiling reveals matrisome alteration as a key feature of ovarian cancer progression. Cancers 2019;11:1513.
44. Kuhn E, Kurman RJ, Vang R, Sehdev AS, Han G, Soslow R, et al. TP53 mutations in serous tubal intraepithelial carcinoma and concurrent pelvic high-grade serous carcinoma–evidence supporting the clonal relationship of the two lesions. J Pathol 2012;226:421–6.
45. Domcke S, Sinha R, Levine DA, Sander C, Schultz N. Evaluating cell lines as tumour models by comparison of genomic profiles. Nat Commun 2013;4:2126.
46. Sanchez-Diaz PC, Chang JC, Moses ES, Dao Tu, Chen Y, Hung JY. Ubiquitin carboxyl-terminal esterase L1 (UCHL1) is associated with stem-like cancer cell functions in pediatric high-grade glioma. PLoS One 2017;12:e0176879.
47. Hussain S, Bedekovics T, Ali A, Zaid O, May DG, Roux KJ, et al. A cysteine near the C-terminus of UCH-L1 is dispensable for catalytic activity but is required to promote AKT phosphorylation, eIF4F assembly, and malignant B-cell survival. Cell Death Discov 2019;5:152.
48. Ilic A, Lu S, Bhatia V, Begum F, Klonisch T, Agarwal P, et al. Ubiquitin C-terminal hydrolase isozyme L1 is associated with shelterin complex at interstitial telomeric sites. Epigenetics Chromatin 2017;10:54.
49. Zimmermann J, Erdmann D, Lalande I, Grossenbacher R, Noorani M, Fürst P. Proteasome inhibitor induced gene expression profiles reveal overexpression of transcriptional regulators ATF3, GADD153 and MAD1. Oncogene 2000;19: 2913–20.
50. Padmanabhan A, Vuong SA, Hochstrasser M. Assembly of an evolutionarily conserved alternative proteasome isoform in human cells. Cell Rep 2016;14: 2962–74.
51. Chui MH, Doodnauth SA, Erdmann N, Tiedemann RE, Sircoulomb F, Drapkin R, et al. Chromosomal instability and mTORC1 activation through PTEN loss contribute to proteotoxic stress in ovarian carcinoma. Cancer Res 2019;79: 5536–49.
52. Su KH, Dai C. mTORC1 senses stresses: coupling stress to proteostasis. Bioessays 2017;39:1600268.
53. Poondla N, Chandrasekaran AP, Kim K-S, Ramakrishna S. Deubiquitinating enzymes as cancer biomarkers: new therapeutic opportunities? BMB Rep 2019; 52:181–9.
54. Sacco JJ, Coulson JM, Clague MJ, Urbé S. Emerging roles of deubiquitinases in cancer-associated pathways. IUBMB Life 2010;62:140–57.
55. Bedekovics T, Hussain S, Feldman AL, Galardy PJ. UCH-L1 is induced in germinal center B cells and identifies patients with aggressive germinal center diffuse large B-cell lymphoma. Blood 2016;127:1564–74.
56. Xiang T, Li L, Yin X, Yuan C, Tan C, Su X, et al. The ubiquitin peptidase UCHL1 induces G0/G1 cell cycle arrest and apoptosis through stabilizing p53 and is frequently silenced in breast cancer. PLoS One 2012;7:e29783.
57. D'Arcy P, Brnjic S, Olofsson MH, Fryknäs M, Lindsten K, De Cesare M, et al. Inhibition of proteasome deubiquitinating activity as a new cancer therapy. Nat Med 2011;17:1636–40.
58. Alexandrova EM, Marchenko ND. Mutant p53 - heat shock response oncogenic cooperation: a new mechanism of cancer cell survival. Front Endocrinol 2015;6:53.
59. Sicari D, Fantuz M, Bellazzo A, Valentino E, Apollonio M, Pontisso I, et al. Mutant p53 improves cancer cells' resistance to endoplasmic reticulum stress by sustaining activation of the UPR regulator ATF6. Oncogene 2019;38:6184–95.
60. Schmidt RM, Schessner JP, Borner GH, Schuck S. The proteasome biogenesis regulator Rpn4 cooperates with the unfolded protein response to promote ER stress resistance. Elife 2019;8:e43244.
61. Lü S, Chen Z, Yang J, Chen Li, Gong S, Zhou H, et al. Overexpression of the PSMB5 gene contributes to bortezomib resistance in T-lymphoblastic lymphoma/leukemia cells derived from Jurkat line. Exp Hematol 2008;36:1278–84.
62. Rowinsky EK, Paner A, Berdeja JG, Paba-Prada C, Venugopal P, Porkka K, et al. Phase 1 study of the protein deubiquitinase inhibitor VLX1570 in patients with relapsed and/or refractory multiple myeloma. Invest New Drugs 2020;38:1448–53.